

Two-dimensional simulation of the spin-flip in the Kapitza-Dirac effect

Ping Ge,¹ Sven Ahrens,^{1,*} and Baifei Shen^{1,†}

¹*Shanghai Normal University, Shanghai 200234, China*

Many calculations in strong field quantum field theory are carried out by using a simple field geometry, often neglecting the spacial field envelope. In this article, we simulate the electron diffraction quantum dynamics of the Kapitza-Dirac effect in a Gaussian beam standing light wave. The two-dimensional simulation is computed in a relativistic framework, by solving the Dirac equation with the fast Fourier transform split operator method. Except the numerical propagation method, our results are obtained without applying approximations and demonstrate that a spin-flip in the Kapitza-Dirac effect is possible.

I. INTRODUCTION

Spin effects for free electrons can be facilitated in present day strong laser fields [1–8]. One particular variation of spin-laser interaction of electrons is the Kapitza-Dirac effect [9, 10], for which spin effects are predicted [11–14], in a scenario similar to Bragg scattering [15–17]. The setup of Kapitza-Dirac scattering, in which an electron traverses a standing light wave, formed by two counterpropagating beams, can be tailored to be sensitive to the spin polarization of the incoming electron [18–24]. Therewith the effect is allowing for a laser based Stern-Gerlach type spin observation [25–27], in form of an induced Compton scattering process [21, 28], being a fundamental photon-only interaction. Experiments in the Bragg regime exist [29], even with observing the cancellation of the interaction at parameters, where spin effects are expected [30].

Most theoretical descriptions of the Kapitza-Dirac effect implement the standing wave potential of the external field by two counterpropagating plane waves, where the field's width and longitudinal polarization component is neglected. As Gaussian beam solutions [31] can be considered to be more realistic than a plane wave approach, we were accounting for the Gaussian beam influence in a recent study on spin-dynamics in Kapitza-Dirac scattering [32]. Still, in order to solve the problem analytically, rough approximations were imposed on the plane wave approach. In order to solve the relativistic equations of motion of the Dirac equation in the perturbative approach, a superposition of a discrete set of plane waves was used in [32]. Naturally, the question arises, whether the approximations of the standing wave vector potential within a perturbative solution technique are sufficiently accurate. In this article, we solve the quantum dynamics of the electron wave function on a two-dimensional grid, by using an Fast-Fourier-transform (FFT) split-operator method [33, 34]. Within this method, the Gaussian beam potential can be implemented exactly, such that no approximations need to be applied to the external field. This work is thus a demonstration of spin-flip dynamics

of an electron in the Kapitza-Dirac effect on the basis of a relativistic, two-dimensional simulation, in which the Dirac equation is evolved numerically.

Our article is organized as follows. In section II, we discuss the simulation setup, by introducing the Gaussian laser beam (section II A), the relativistic quantum description (section II B) and the initial condition of the electron quantum state (section II C). We also mention details about simulation parameter configuration, as well as the numerical procedure of the Q-Wave library in section II D. We then present the simulation results in section III. The results include the demonstration of electron diffraction dynamics as in the Kapitza-Dirac effect in (section III A), with displaying the spin properties of the quantum dynamics in section III B. We finally summarize our investigation and give an outlook on possible, related topics in section IV.

II. SETUP OF OUR INVESTIGATION

For our computer simulation we make use of the Q-Wave utility [34]. Q-Wave is an advanced computer code, available as C++ library, which implements the FFT split-operator method, among other numerical algorithms [35]. It provides the building blocks for numerically propagating wave functions in time. In the following, we describe the physical setup which we investigate by using Q-Wave. Regarding the units in our article, we write m for the electron rest mass, c for the vacuum speed of light, \hbar for the reduced Planck constant and q for the elementary charge in a Gaussian unit system.

A. Gaussian beam configuration

We first describe the vector potential of our simulation. A Gaussian beam shaped standing light wave can be formed from two Gaussian beams [36], where reference [36] builds on a solution based on an angular spectrum representation of plane waves. The laser beam is propagating along the x -axis, in our two-dimensional simulation, where the simulation area is aligned in the x - y plane. For the geometry in this article, the Gaussian

* ahrens@shnu.edu.cn

† bfshen@shnu.edu.cn

beam is denoted as

$$A_{x,d} = -2dA_0 \frac{w_0}{w} \epsilon \frac{y}{w} \exp\left(-\frac{r^2}{w^2}\right) \cos\left(\phi_{G,d}^{(1)}\right) \quad (1a)$$

for the longitudinal polarization component and

$$A_{y,d} = -A_0 \frac{w_0}{w} \exp\left(-\frac{r^2}{w^2}\right) \sin\left(\phi_{G,d}\right) \quad (1b)$$

for the transverse polarization component of the vector potential in Coulomb gauge [37]. The potentials in Eq.(1) further contain the phases

$$\phi_{G,d} = \omega t - dk_L x + \tan^{-1}\left(\frac{dx}{x_R}\right) - \frac{dxr^2}{x_R w^2} \quad (2a)$$

$$\phi_{G,d}^{(1)} = \phi_{G,d} + \tan^{-1}\left(\frac{dx}{x_R}\right) \quad (2b)$$

and the symbol w represents the x -dependent beam waist

$$w(x) = w_0 \sqrt{1 + \frac{x^2}{x_R^2}}. \quad (3)$$

We choose the Gaussian beam to oscillate with frequency $\omega = 0.1 mc^2/\hbar$, corresponding to the wave number $k_L = 0.1 mc/\hbar$ and wavelength $\lambda = 2\pi k_L$. Reference [36] introduces the beam focus as $\omega_0 = 1/(k_L \epsilon)$, where we set the beam divergences as $\epsilon = 0.02$. The Rayleigh length of the Gaussian beam is given by $x_R = k_L \omega_0^2/2$.

The index d in Eqs. (1) parameterizes the propagation direction of the laser beam, where the two possible directions $d \in \{-1, 1\}$ correspond to the left or right moving direction, respectively. In the Kapitza-Dirac effect, the standing wave vector potential can be formed from two counterpropagating beams as

$$\mathbf{A} = \sum_d (A_{x,d} \mathbf{e}_x + A_{y,d} \mathbf{e}_y). \quad (4)$$

In Fig. 1 we display the field \mathbf{A} as it appears after a quarter laser period $t = \omega/(2\pi)$. In contrast to previous theoretical investigations, transverse and longitudinal polarization are both computed without applying approximations here, with a finite beam width and a longitudinal polarization component.

B. Relativistic quantum theory

Since the laser field in our simulation is strong and the initial electron momentum of electron is $1mc$, we use a relativistic spin 1/2 quantum theory for the description of our simulation, given by the electromagnetically coupled Hamiltonian of the Dirac equation

$$H = c \left(\mathbf{p} - \frac{q}{c} \mathbf{A} \right) \cdot \boldsymbol{\alpha} + q\phi + \beta mc^2. \quad (5)$$

The gauge potential \mathbf{A} has been introduced in subsection A, where set the scalar potential $\phi = 0$ in our code. The

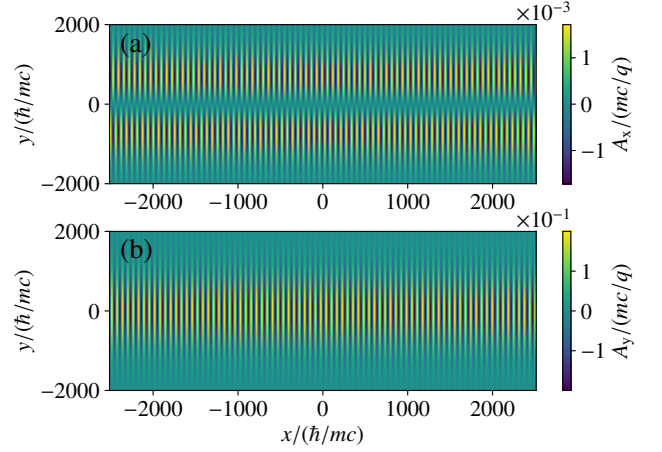


FIG. 1. Vector potential of a Gaussian beam standing wave in our simulation, according to Eq. (4). The longitudinal (1a) and transverse (1b) polarization component of the laser beam are displayed at the upper and lower panel, respectively. We use the laser parameters $A_0 = 0.1 mc/q$ for the field amplitude, $k_L = 0.1 mc/\hbar$ for the wave number and $\epsilon = 0.02$ for the beam divergence, in the Gaussian beam, displayed after at a quarter laser period $t = \omega/(2\pi)$. In our two-dimensional simulation area, the electron passes the Gaussian beam from bottom to top, along the y -direction.

objects $\boldsymbol{\alpha}$ and $\boldsymbol{\beta}$ are the 4×4 Dirac matrices in standard representation (also called Dirac representation). We write the energy eigenvalue relations in momentum space as

$$H \psi_z^s(\mathbf{p}) = E_p \psi_z^s(\mathbf{p}), \quad (6)$$

with the positive plane wave solutions of the Dirac equation

$$\psi_z^s(\mathbf{p}) = u_z^s(\mathbf{p}) e^{i\mathbf{r} \cdot \mathbf{p}/\hbar}, \quad (7)$$

where we denote the bi-spinors $u_z^s(\mathbf{p})$ as

$$u_z^s(\mathbf{p}) = \sqrt{\frac{E_p + mc^2}{2mc^2}} \begin{pmatrix} \chi_z^s \\ \frac{c\boldsymbol{\sigma} \cdot \mathbf{p}}{E_p + mc^2} \end{pmatrix}. \quad (8)$$

In Eqs.(6)-(8), the parameter $s \in \{+, -\}$ is indexing the state of the electron spin, where the index z indicates the quantization axis for the spin orientation to be along the z -axis. We also write $E_p = \sqrt{m^2 c^4 + c^2 \mathbf{p}^2}$ for the relativistic energy, $\mathbf{p} = p_x \cdot \mathbf{e}_x + p_y \cdot \mathbf{e}_y$ for the momentum vector and $\boldsymbol{\sigma}$ for the vector of Pauli matrices.

C. The initial electron quantum state

According to the Q-Wave simulation package [34], the wave packet of the electron is initialized as a Gaussian wave packet, in our two-dimensional simulation, with the

density distribution

$$\rho(\mathbf{p}) = \frac{1}{\sqrt{2\pi}\sigma_p} \exp \left[- \left(\frac{\mathbf{p} - \mathbf{p}_0}{2\sigma_p} \right)^2 - i \frac{\mathbf{r}_0 \cdot \mathbf{p}}{\hbar} \right] \quad (9)$$

in momentum space. The Gaussian distribution is centered at momentum \mathbf{p}_0 , with wave packet size parameter σ_p . The second term in the exponential implies the particle's position at \mathbf{r}_0 . The wave function in momentum space is set up as

$$\varphi_z^s(\mathbf{p}, 0) = u_z^s(\mathbf{p})\rho(\mathbf{p}), \quad (10)$$

on the basis of the distribution (9). In position space, the wave function Ψ_z is then implied by the two-dimensional Fourier transformations

$$\varphi_z^s(\mathbf{p}, t) = \frac{1}{2\pi\hbar} \int \Psi_z^s(\mathbf{r}, t) \exp \left(- \frac{i\mathbf{r} \cdot \mathbf{p}}{\hbar} \right) d^2r \quad (11a)$$

$$\Psi_z^s(\mathbf{r}, t) = \frac{1}{2\pi\hbar} \int \varphi_z^s(\mathbf{p}, t) \exp \left(\frac{i\mathbf{r} \cdot \mathbf{p}}{\hbar} \right) d^2p. \quad (11b)$$

D. Numerical propagation and simulation parameters

The Q-Wave library provides numerical algorithms to solve the time-evolution of quantum wave function in multiple time steps. We make use of the Fourier split operator method [34] for which the a time step with time stepping Δt can be denoted as a mapping of the wave function $\Psi(r, t)$ to the wave function $\Psi(r, t + \Delta t)$ at a later point in time by

$$\Psi(\mathbf{r}, t + \Delta t) = \mathbf{U}(t + \Delta t, t)\Psi(\mathbf{r}, t). \quad (12)$$

The solution is implemented such that the time evolution operator $\mathbf{U}(t + \Delta t, t)$ corresponds to the computation of the exponential

$$\mathbf{U}(t_i + \Delta t, t_i) = \hat{T} \exp \left[- \frac{i}{\hbar} \int_{t_i}^{t_i + \Delta t} H(t') dt' \right] \quad (13)$$

with time ordering operator \hat{T} and Hamiltonian Eq. (5) of our system.

In the following we will introduce specific values of parameters, which are set in the simulation. We carry out our simulation on a grid with 2048×128 grid points, with simulation area width 80λ and height 40λ , in the x and y direction, respectively. Along the x -axis we set the minimum and maximum simulation box limits $x_{\min} = -40\lambda$ and $x_{\max} = 40\lambda$. For the y -axis, we require the electron wave packet to be centered in our simulation area, initially and during the simulation, as sketched in Fig. 2. We choose the initial simulation box limits as $y_{\min}(0) = -160\lambda$ and $y_{\max}(0) = -120\lambda$, approximately 15 half beam waists w_0 away from the laser beam center.

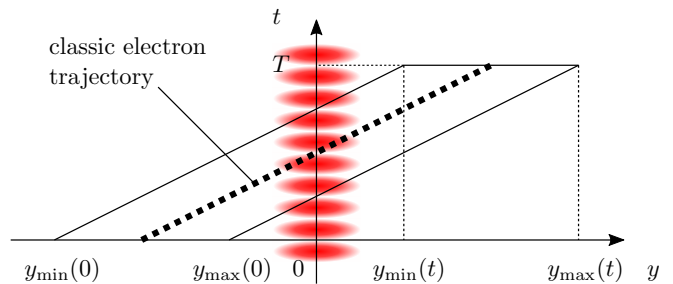


FIG. 2. Illustration of the simulation box limits and electron location along the y -direction. The red, oval shaped shades symbolize the laser beam position over time, located at $y = 0$. Along the y -direction, the simulation box size equals 40λ with initial minimum and maximum positions $y_{\min}(0) = -160\lambda$ and $y_{\max}(0) = -120\lambda$, respectively, at time $t = 0$. The electron is initially placed in the simulation box center, at $y = -140\lambda$ and moves approximately along the classical electron trajectory $y_{\text{CET}}(t)$, as given in Eq. (17), which we indicate by the thick, dotted line. We shift the simulation box every 2805 time steps by $9.8 \cdot 10^3 \hbar/mc$ (177 times in total) until the simulation box limits reach the coordinates $y_{\min}(T) = 120\lambda$ and $y_{\max}(T) = 160\lambda$ at time $t = T$. In the supplemental material, we provide an animation of the vector potential as in Fig. 1, within the moving bounds of the parameterized y -axis, as sketched here.

The electron's initial position along the y -direction is in the simulation box center at $y = -140\lambda$. Regarding the electron's momentum, we set the momentum $p_x = -\hbar k_L$ along x -axis, to meet the Bragg condition for the two-photon Kapitza-Dirac effect [11, 12, 38]. The y -component of the electron momentum is implied by the requirement for spin effects in the Kapitza-Dirac effect [12, 21, 39] to be $p_y = 1mc$. The momentum parameter \mathbf{p}_0 for the initial electron state in Eq. (9) is therefore assuming the value

$$\mathbf{p}_0 = \begin{pmatrix} -\hbar k_L \\ mc \end{pmatrix}, \quad (14)$$

with inclination angle of the Bragg condition

$$\vartheta = \arctan(|p_x|/|p_y|). \quad (15)$$

Requiring that the electron needs to move through the coordinate origin, this also implies the initial electron position along the laser beam propagation direction to be $x = 14\lambda$, such that the initial position vector in Eq. (9) reads

$$\mathbf{r}_0 = \begin{pmatrix} 14\lambda \\ -140\lambda \end{pmatrix}. \quad (16)$$

The momentum spread of the electron we set to $\sigma_p = \hbar k_L/200$, corresponding to an electron wave function extension on the order of 100 wave laser wave lengths. Concerning the simulation time, we mention that the significant y -component of the electron momentum (14) implies

the approximate classical electron velocity $v_y = c/\sqrt{2}$, with the corresponding y -component of the classical electron trajectory

$$y_{\text{CET}}(t) = -140\lambda + \frac{1}{\sqrt{2}}ct. \quad (17)$$

This implies the traveling time $\tilde{T} = 280\lambda\sqrt{2}/c = 2.5 \cdot 10^4 \hbar/(mc^2)$ for the electron to reach $y = 140\lambda$. Further, we choose the time stepping $\Delta t = 0.05 \hbar/mc^2$, for resolving the oscillation of the mass term βmc^2 in the Dirac equation. Therefore, regarding the electron velocity component v_y , we need to shift the simulation area by 5 grid points along the y -direction every 2805 time steps, to keep the electron wave function centered in the simulation box, as illustrated in Fig. 2. After 177 grid rearrangements we reach the total simulation time $T = \Delta t \times 2805 \times 177 \approx \tilde{T}$.

Regarding the external field, we mention again the Gaussian beam parameters of Eqs. (1) and (2) for the vector potential from section II A, as $\omega = 0.1\hbar/mc$ for the laser angular frequency, with wave number $k_L = 0.1mc/\hbar$, $A_0 = 0.1mc/q$ for the field amplitude and $\epsilon = 0.02$ for the beam divergence. We remark, that for technical reasons, we introduce a shift between the kinetic and canonical momentum of the wave packet by employing a gauge with constant vector potential $A_m = 1.0mc/q$ in the y -axis of Eq. (4) in our numeric implementation.

III. SIMULATION RESULTS AND ANALYSIS

After the introduction of the external field (section II A), relativistic quantum theory (section II B), initial quantum state (section II C) and simulation parameters (section II D) we are now turning to the discussion of the simulation results and its analysis.

A. Motion of the electron probability density

We display the electron probability density

$$|\Psi_z^+(\mathbf{r}, t)|^2 = [\Psi_z^+(\mathbf{r}, t)]^\dagger \Psi_z^+(\mathbf{r}, t) \quad (18)$$

at initial time $t = 0$ in Fig. 3(a) and after propagation for the simulation time T in Fig. 3(b), where all parameters are used as described in section II D. For illustration of the process, which takes place between the situation in Fig. 3(a) and Fig. 3(b), we compute the y -averaged density

$$\Phi(x, t) = \int_{y_{\min}(t)}^{y_{\max}(t)} |\Psi(x, y, t)|^2 dy \quad (19)$$

and display it in Fig. 4. We observe in Fig. 4 that the electron is moving from the right to the left, corresponding the the initially set and the expected electron

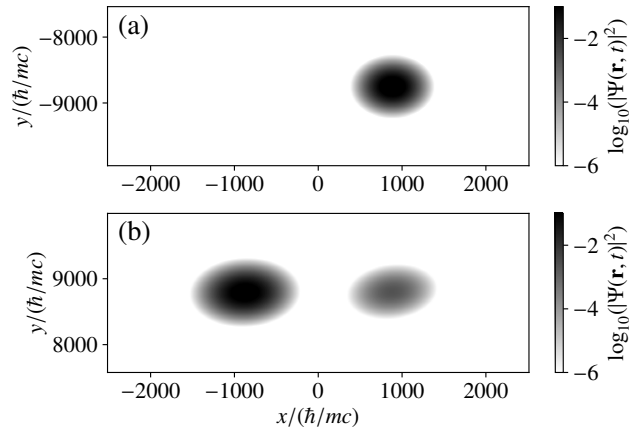


FIG. 3. Probability density of the electron at initial and final time. The upper panel displays the initial electron probability density $|\Psi^+(\mathbf{r}, 0)|^2$, at time $t = 0$ according to Eq. (18), which corresponds to the initial condition (9). The lower panel shows the electron probability $|\Psi^+(\mathbf{r}, T)|^2$, at final time $t = T$. Due to the co-moving simulation area, as illustrated in Fig. 2, the electron remains centered along the vertical and only moves from the right to the left. The light gray peak on the right of the lower panel is the diffracted portion of the electron wave function.

positions along the x -axis at $x = 14\lambda$ and $x = -14\lambda$, respectively. However, due to the interaction of the electron with the laser beam at time $T/2$, a diffracted part appears in the central region of Fig. 4, which moves from the center to the right, displaying the Kapitza-Dirac effect. The dynamics of the electron in Fig. 4 explains the motion of the initial location of the electron on the right in Fig. 3(a) to the left in Fig. 3(b). Accordingly, the gray peak at the right of Fig. 3(b) corresponds to the diffracted electron beam. Note, that the electron is not showing any significant motion along the y -axis in Fig. 3, as we are moving the simulation box with the electron along the y -direction, corresponding to the sketch in Fig. 2. An animation of the position space dynamics of the electron density $|\Psi(x, y, t)|^2$ as in Fig. 3 is provided in the supplemental material.

B. Investigation of spin resolved quantum dynamics

Having demonstrated quantum dynamics as predicted by the Kapitza-Dirac effect, we want to further present spin effects as discussed in [12, 21, 32], where the references imply that the spin is rotating around the magnetic field direction of the linearly polarized standing light wave. In our case, the magnetic field is pointing in the z -direction, implying only a phase change for spin- z polarized electrons. We therefore construct the x -polarized

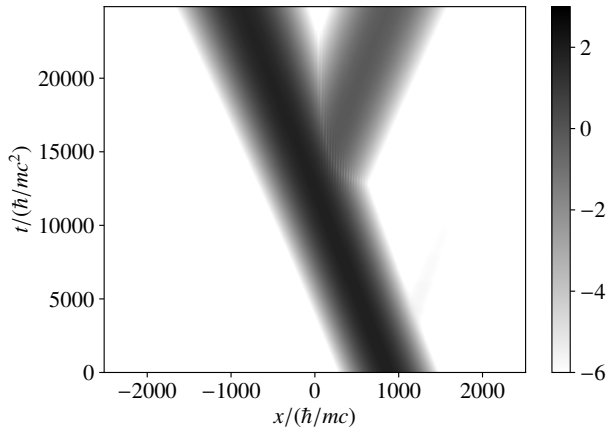


FIG. 4. The y -integrated probability density $\Phi(x, t)$ as in Eq. (19) over time. One can see that the electron moves from the right to the left, where the diffracted beam forms at the center of the figure and moves to the right, demonstrating quantum dynamics as in the Kapitza-Dirac effect. The lower leg of the y -shaped figure corresponds to the peak of the initial state in Fig. 3(a), whereas the two upper legs correspond to the two final peaks in Fig. 3(b).

wavefunction

$$\varphi_x^s(\mathbf{p}, t) = \frac{1}{\sqrt{2}} [\varphi_z^+(\mathbf{p}, t) + s\varphi_z^-(\mathbf{p}, t)] \quad (20)$$

from the z -polarized solutions, with $s \in \{+, -\}$. Further, with the use of x -polarized spinors

$$u_x^s(\mathbf{p}) = \frac{1}{\sqrt{2}} [u_z^+(\mathbf{p}) + su_z^-(\mathbf{p})], \quad (21)$$

we compute the transition amplitude

$$c^{s_f, s_i}(\mathbf{p}, t) = \langle u_x^{s_f}(\mathbf{p}) | \varphi_x^{s_i}(\mathbf{p}, t) \rangle \quad (22)$$

from initial spin s_i to final spin s_f with respect to the x -polarization axis. Note, that the quantities (20) and (22) are given in momentum space, since one can easily specify the spin in terms of the bi-spinors (8). The momentum space wave function (20) is implied from the simulated position space wave function $\Psi(\mathbf{r}, t)$ by the Fourier transform (11a). The absolute value squared of the transition (22) is displayed in Fig. 5 at time T , the end of the simulation period. Thus, Fig. 5 corresponds to the momentum space situation of the position space density in Fig. 3(b).

The prominent peak on the left in Fig. 5(a) corresponds to the initial condition (9) with momentum coordinates (14) and remains merely unchanged during the course of the simulation. It corresponds to the electron's motion from the right to the left in Fig. 4. In contrast, the right peak Fig. 5(a) and the peak in Fig. 5(b), arise due to the interaction of the electron with the laser, and

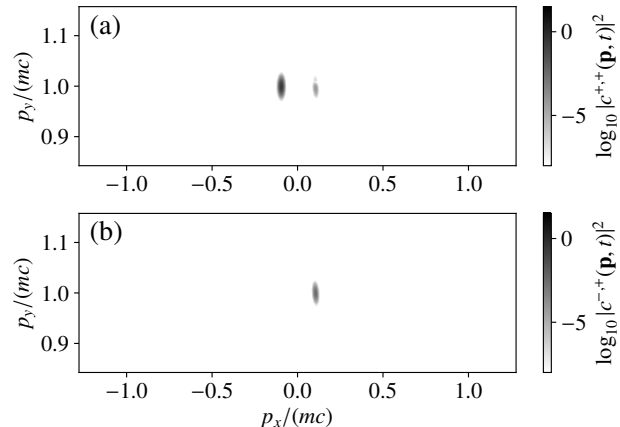


FIG. 5. Electron spin projection $|c^{s_f}(\mathbf{p}, T)|^2$ along the x -polarization direction according to Eq. (22) at the end of the simulation. The projection direction s_f is positive in the upper panel and negative in the lower panel. Since the spin is determined in momentum space, this figure corresponds to the spin-resolved momentum space probability of the final electron density in Fig. 3(b). We observe that on diffraction of the initial electron beam on the left peak of the upper panel, a diffracted portion of the wave function appears two photon momenta $2k_L e_x$ to the right. The spin $-x$ component of the diffracted beam (lower panel) appears larger than the spin $+x$ component (upper panel, right peak).

correspond to the right moving Bragg peak in Fig. 4. Initial condition and the appearance of the Bragg peak over time can be viewed in detail in the animations of Fig. 5 in the supplemental material. The figure allows for the association of spin-polarization with the moving and diffracted portions of the electron wave function. While the left moving electron beam is purely polarized in the positive x direction (as implied by the initial condition), the diffracted beam depicts a contribution with $s^f = +$ as well as $s^f = -$. Note, that the peak of the negative spin- x polarization appears to be more pronounced than the peak of the positive spin- x polarization.

For quantifying the spin amplitude, we plot the wave function's probability density in momentum space

$$\Upsilon^0(p_x) = |\varphi_z^+(p_x, mc, T)|^2 = [\varphi_z^+(p_x, mc, T)]^\dagger \varphi_z^+(p_x, mc, T) \quad (23)$$

together with the spin projections

$$\Upsilon^{s_f}(p_x) = |c^{s_f, +}(p_x, mc, T)|^2 \quad (24)$$

at y -axis position $p_y = mc$ in Fig. 6. We observe the initial beam on the left and the diffracted beam on the right, as we have identified them already in Fig. 5. One can see, that the projection of the spin $+x$ -polarization Υ^+ is coinciding with the probability density Υ^0 for the initial beam. On contrary, it is the projection of the spin $-x$ -polarization Υ^- , which matches

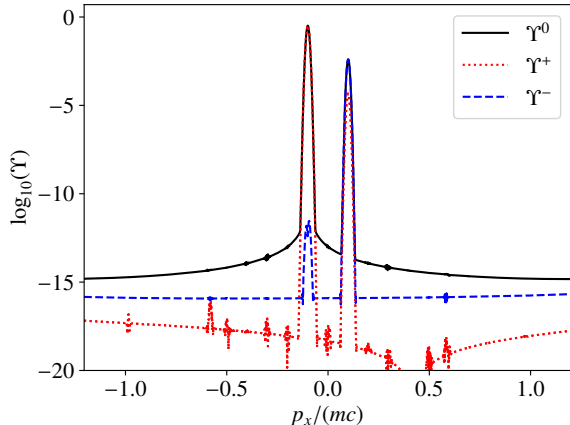


FIG. 6. Spin resolved momentum space density of the electron along the p_x -axis at final simulation time $t = T$. Displayed are the probability density Υ^0 , according to Eq. (23) and the spin $+x$ (Υ^+) and spin $-x$ (Υ^-) projections according to Eq. (24). One can see that the momentum density Υ^0 of the initial electron beam (left peak at $p_x = -\hbar k_L$) is coinciding with the spin $+x$ component Υ^+ . However, the diffracted beam (right peak at $p_x = \hbar k_L$), is coinciding with the spin $-x$ component Υ^- . The spin $+x$ component in the diffracted beam is smaller by about two orders of magnitude and demonstrates a spin-flip in the Kapitza-Dirac effect.

the probability density Υ^0 in the diffracted beam. In numbers, the diffracted beam's spin $+x$ polarization amplitude is $\Upsilon^+(0.1mc) = 4.6 \times 10^{-5}$, whereas the spin $-x$ -polarization amplitude $\Upsilon^-(0.1mc) = 3.9 \times 10^{-3}$ is larger by about two orders of magnitude. We thus conclude clear spin-flip dynamics along the x -spin polarization axis from our simulation, which agrees with the predictions in references [12] and [21]. A time-evolution of $|\varphi_z^+(p_x, mc, t)|^2$ and $|c^{sf,+}(p_x, mc, t)|^2$ of the wave function's in-field dynamics in a similar fashion as in Fig. 6

is provided in the supplemental material of this article.

IV. CONCLUSION AND OUTLOOK

In this article, we have carried out a two-dimensional, relativistic simulation of the Kapitza-Dirac effect, by using an FFT split-operator method. The standing wave laser beam is modelled by two counterpropagating Gaussian beams and thus goes beyond the plane wave ansatz of previous investigations. Likewise, the electron wave function is implemented as a finite-size Gaussian wave packet. Within the used parameters, we are able to show a Bragg peak in the Bragg regime, which is the characteristic aspect of the Kapitza-Dirac effect. Further, we have demonstrated a spin-flip along the x -polarization axis of the electron spin, implying that formerly discussed spin effects are theoretically possible in Kapitza-Dirac scattering, which we conclude without applying approximations.

It will be interesting to see, how spin effects in the Kapitza-Dirac effect are changing with parameters, in particular with regard to the photon momentum $\hbar k_L$ and the beam divergence ϵ . The recently aroused question about the influence of the longitudinal beam polarization component of the Gaussian beam on the spin dynamics will be of relevance [32, 40]. Further questions, which might be of interest in two-dimensional Kapitza-Dirac scattering might be the role of negative solutions in relativistic quantum dynamics their behavior with additional external fields added.

ACKNOWLEDGMENTS

We thank Heiko Bauke for providing the Q-Wave library for implementing quantum computations. The work was supported by the National Natural Science Foundation of China (Grants No. 11975155 and 11935008).

-
- [1] Y.-Y. Chen, P.-L. He, R. Shaisultanov, K. Z. Hatsagortsyan, and C. H. Keitel, Polarized Positron Beams via Intense Two-Color Laser Pulses, *Phys. Rev. Lett.* **123**, 174801 (2019).
 - [2] Y.-F. Li, R. Shaisultanov, K. Z. Hatsagortsyan, F. Wan, C. H. Keitel, and J.-X. Li, Ultrarelativistic Electron-Beam Polarization in Single-Shot Interaction with an Ultraintense Laser Pulse, *Phys. Rev. Lett.* **122**, 154801 (2019).
 - [3] Y.-F. Li, Y.-Y. Chen, W.-M. Wang, and H.-S. Hu, Production of Highly Polarized Positron Beams via Helicity Transfer from Polarized Electrons in a Strong Laser Field, *Phys. Rev. Lett.* **125**, 044802 (2020).
 - [4] M. Wen, M. Tamburini, and C. H. Keitel, Polarized Laser-WakeField-Accelerated Kiloampere Electron Beams, *Phys. Rev. Lett.* **122**, 214801 (2019).
 - [5] D. Del Sorbo, D. Seipt, T. G. Blackburn, A. G. R. Thomas, C. D. Murphy, J. G. Kirk, and C. P. Ridgers, Spin polarization of electrons by ultraintense lasers, *Phys. Rev. A* **96**, 043407 (2017).
 - [6] D. V. Karlovets, Radiative polarization of electrons in a strong laser wave, *Phys. Rev. A* **84**, 062116 (2011).
 - [7] K. van Kruining, F. Mackenroth, and J. B. Götze, Radiative spin polarization of electrons in an ultrastrong magnetic field, *Phys. Rev. D* **100**, 056014 (2019).
 - [8] Y.-F. Li, Y.-Y. Chen, K. Z. Hatsagortsyan, A. Di Piazza, M. Tamburini, and C. H. Keitel, Strong signature of one-loop self-energy in polarization resolved nonlinear Compton scattering, *Phys. Rev. D* **107**, 116020 (2023).
 - [9] P. L. Kapitza and P. A. M. Dirac, The reflection of electrons from standing light waves, *Math. Proc. Cambridge Philos. Soc.* **29**, 297 (1933).
 - [10] D. L. Freimund, K. Aflatooni, and H. Batelaan, Observation of the Kapitza-Dirac effect, *Nature (London)* **413**,

- 142 (2001).
- [11] S. Ahrens, H. Bauke, C. H. Keitel, and C. Müller, Spin Dynamics in the Kapitza-Dirac Effect, *Phys. Rev. Lett.* **109**, 043601 (2012).
- [12] S. Ahrens, H. Bauke, C. H. Keitel, and C. Müller, Kapitza-Dirac effect in the relativistic regime, *Phys. Rev. A* **88**, 012115 (2013).
- [13] M. M. Dellweg, H. M. Awwad, and C. Müller, Spin dynamics in Kapitza-Dirac scattering of electrons from bichromatic laser fields, *Phys. Rev. A* **94**, 022122 (2016).
- [14] R. Erhard and H. Bauke, Spin effects in Kapitza-Dirac scattering at light with elliptical polarization, *Phys. Rev. A* **92**, 042123 (2015).
- [15] W. H. Bragg and W. L. Bragg, The reflection of X-rays by crystals, *Proc. R. Soc. London. Series A* **88**, 428 (1913).
- [16] H. Batelaan, The Kapitza-Dirac effect, *Contemp. Phys.* **41**, 369 (2000).
- [17] H. Batelaan, *Colloquium* : Illuminating the Kapitza-Dirac effect with electron matter optics, *Rev. Mod. Phys.* **79**, 929 (2007).
- [18] M. M. Dellweg and C. Müller, Spin-Polarizing Interferometric Beam Splitter for Free Electrons, *Phys. Rev. Lett.* **118**, 070403 (2017).
- [19] S. Ahrens, Electron-spin filter and polarizer in a standing light wave, *Phys. Rev. A* **96**, 052132 (2017).
- [20] M. M. Dellweg and C. Müller, Controlling electron spin dynamics in bichromatic Kapitza-Dirac scattering by the laser field polarization, *Phys. Rev. A* **95**, 042124 (2017).
- [21] S. Ahrens, Z. Liang, T. Čadež, and B. Shen, Spin-dependent two-photon Bragg scattering in the Kapitza-Dirac effect, *Phys. Rev. A* **102**, 033106 (2020).
- [22] S. McGregor, W. C.-W. Huang, B. A. Shadwick, and H. Batelaan, Spin-dependent two-color Kapitza-Dirac effects, *Phys. Rev. A* **92**, 023834 (2015).
- [23] A. Ebadati, M. Vafaei, and B. Shokri, Four-photon Kapitza-Dirac effect as an electron spin filter, *Phys. Rev. A* **98**, 032505 (2018).
- [24] A. Ebadati, M. Vafaei, and B. Shokri, Investigation of electron spin dynamic in the bichromatic Kapitza-Dirac effect via frequency ratio and amplitude of laser beams, *Phys. Rev. A* **100**, 052514 (2019).
- [25] W. Gerlach and O. Stern, Der experimentelle Nachweis der Richtungsquantelung im Magnetfeld, *Zeitschrift für Physik* **9**, 349 (1922).
- [26] W. Gerlach and O. Stern, Das magnetische Moment des Silberatoms, *Zeitschrift für Physik* **9**, 353 (1922).
- [27] W. Gerlach and O. Stern, Der experimentelle Nachweis des magnetischen Moments des Silberatoms, *Zeitschrift für Physik* **8**, 110 (1922).
- [28] A. H. Compton, A Quantum Theory of the Scattering of X-rays by Light Elements, *Phys. Rev.* **21**, 483 (1923).
- [29] D. L. Freimund and H. Batelaan, Bragg Scattering of Free Electrons Using the Kapitza-Dirac Effect, *Phys. Rev. Lett.* **89**, 283602 (2002).
- [30] J. J. Axelrod, S. L. Campbell, O. Schwartz, C. Turnbaugh, R. M. Glaeser, and H. Müller, Observation of the Relativistic Reversal of the Ponderomotive Potential, *Phys. Rev. Lett.* **124**, 174801 (2020).
- [31] L. D. Dickson, Characteristics of a Propagating Gaussian Beam, *Appl. Opt.* **9**, 1854 (1970).
- [32] S. Ahrens, Z. Guan, and B. Shen, Beam focus and longitudinal polarization influence on spin dynamics in the Kapitza-Dirac effect, *Phys. Rev. A* **105**, 053123 (2022).
- [33] J. W. Braun, Q. Su, and R. Grobe, Numerical approach to solve the time-dependent Dirac equation, *Phys. Rev. A* **59**, 604 (1999).
- [34] H. Bauke and C. H. Keitel, Accelerating the Fourier split operator method via graphics processing units, *Comput. Phys. Commun.* **182**, 2454 (2011).
- [35] R. Beerwerth and H. Bauke, Krylov subspace methods for the Dirac equation, *Computer Physics Communications* **188**, 189 (2015).
- [36] B. Quesnel and P. Mora, Theory and simulation of the interaction of ultraintense laser pulses with electrons in vacuum, *Phys. Rev. E* **58**, 3719 (1998).
- [37] Further details about adjusting the fields in [36] can be found in the appendix of reference [32].
- [38] S. Ahrens, *Investigation of the Kapitza-Dirac effect in the relativistic regime*, Ph.D. thesis, Ruprecht-Karls University Heidelberg (2012), <http://archiv.ub.uni-heidelberg.de/volltextserver/14049/>.
- [39] S. Ahrens and C.-P. Sun, Spin in Compton scattering with pronounced polarization dynamics, *Phys. Rev. A* **96**, 063407 (2017).
- [40] S. Ahrens, C. Zhang, P. Ge, G. W. Y. Li, and B. F. Shen, Perturbative solution approach for computing the two-photon Kapitza-Dirac effect in a Gaussian beam standing light wave, arXiv:2305.12399.